arXiv:1408.0804v1 [cond-mat.str-el] 4 Aug 2014

Excitonic Quasiparticles in a Spin-Orbit Mott Insulator

Jungho Kim,[1] M. Daghofer, [2] A. H. Said, [1] T. Gog,[1] J. van den Brink,[2] G. Khaliullin,[3] B. J. Kim[3,4,*]
[1]*Advanced Photon Source, Argonne National Laboratory, Argonne, Illinois 60439, USA*
[2]*Institute for Theoretical Solid Sate Physics, IFW Dresden, Helmholtzstr. 20, 01069 Dresden, Germany*
[3]*Max Planck Institute for Solid State Research, Heisenbergstraße 1, D-70569 Stuttgart, Germany and*
[4]*Materials Science Division, Argonne National Laboratory, Argonne, IL 60439, USA*

In condensed matter systems, out of a large number of interacting degrees of freedom emerge weakly coupled particles, in terms of which most physical properties are described. For example, Landau quasiparticles[1] (QP) determine all electronic properties of a normal metal. The lack of identification of such QPs is a major barrier for understanding myriad exotic properties of correlated electrons, such as unconventional superconductivity[2] and non-Fermi liquid behaviors.[3] Here, we report the observation of a composite particle in a Mott insulator Sr_2IrO_4—an exciton dressed with magnons–that propagates with the canonical characteristics of a QP: a finite QP residue and a lifetime longer than the hopping time scale. The dynamics of this charge-neutral bosonic excitation mirrors the fundamental process of the analogous one-hole propagation in the background of ordered spins,[4] for which a well-defined QP has never been observed. The much narrower linewidth of the exciton reveals the same intrinsic dynamics that is obscured for the hole and is intimately related to the mechanism of high temperature superconductivity.

The dynamics of a single hole doped into a Mott insulator is one of the unresolved fundamental issues in the physics of high temperature superconductivity in the cuprates.[4–6] In one picture, the single hole forms a coherent quasiparticle (QP) propagating in a medium of ordered spins, which strongly renormalizes the dispersion relations and the mutual interactions of the holes. This spin-polaron picture, supported by numerical approaches, such as quantum Monte-Carlo,[7] exact diagonalization[8] and self-consistent Born approximation (SCBA),[5] naturally connects to the pairing mechanism of pre-existing QPs glued by retarded bosons, analogous to Bardeen-Cooper-Schrieffer mechanism for conventional superconductivity. In a contrasting picture, the phenomenological absence of QPs in angle-resolved photoemission (ARPES)[9–11] and scanning tunneling spectra[12] is argued as due to orthogonality catastrophe,[13] spin-charge separation,[14] and/or localization effects,[15] reflecting the unconventional nature of two-dimensional, strongly interacting fermions, which may support more exotic mechanisms of superconductivity such as the resonating valence bond theory proposed by Anderson.[16]

Motivated by the recent discovery of a new pseudospin-1/2 Heisenberg antiferromagnet on a square lattice, Sr_2IrO_4,[17–22] we demonstrate in this letter a novel experimental approach using resonant inelastic x-ray scattering (RIXS), which is a rapidly evolving tool especially well suited for such 5d transition-metal oxides, to address this longstanding problem. Based on its remarkable similarity to superconducting cuprates in structural,[22] electronic,[17] and magnetic aspects,[20,21] superconductivity has been predicted in Sr_2IrO_4.[23] Although the electron correlation strength in Sr_2IrO_4 has been under much debate,[24–28] questioning the validity of classifying this compound as a Mott insulator, Sr_2IrO_4 shares the same phenomenology that the hole spectral function as measured by ARPES lacks a legitimate QP.[17] This similarity suggests a common origin for the absence of a well-defined QP in the ARPES spectra for two distinct but similar classes of materials. As we shall see, however, Sr_2IrO_4 supports a well-defined QP in another excitation channel, which RIXS is sensitive to and reflects the same dynamics as that of a hole, offering a novel route to studying elementary excitations in correlated oxides.

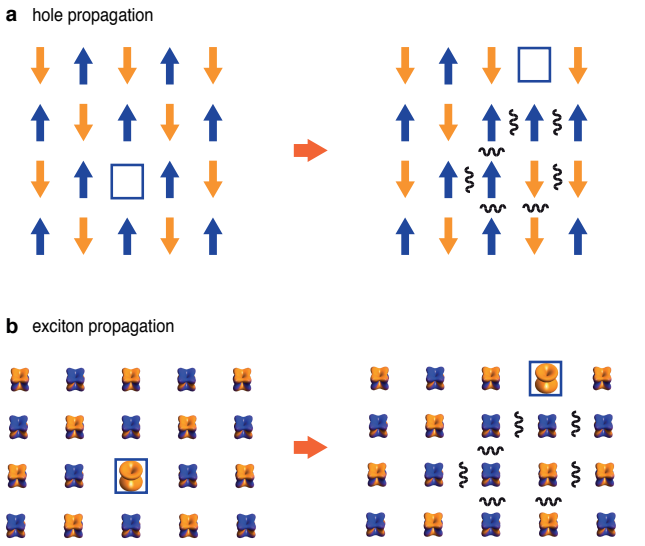

FIG. 1. **Hole vs. exciton propagation in an antiferromagnetic background. a**, a moving hole (blue square) creates a string of excited spins. Black wavy lines indicate pairs of 'misaligned' spins. **b**, an analogous exciton hopping.

In an earlier RIXS study of Sr_2IrO_4, dispersive d-d excitations (or excitons) across the spin-orbit coupling split levels (see Fig. 2a) have been identified and it has been shown that their dispersions can be understood in close analogy to the single hole problem.[20] Figure 1 depicts the

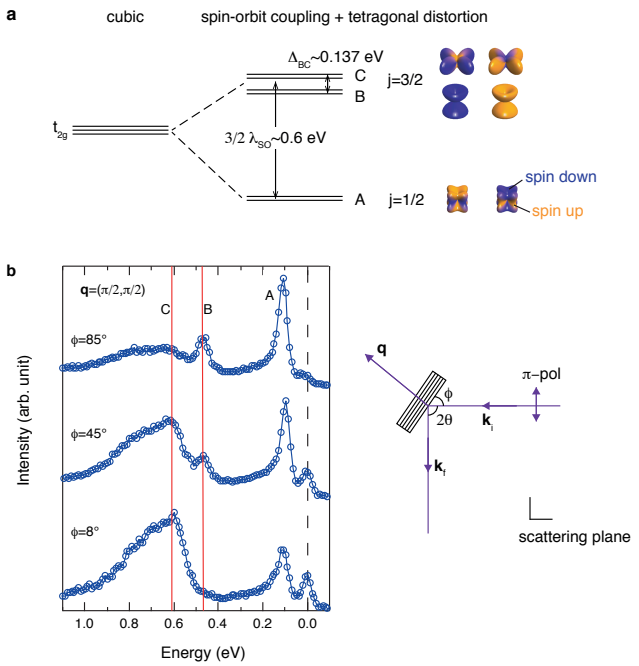

FIG. 2. **RIXS spectra of Sr_2IrO_4. a**, the spin-orbital level scheme of the three Kramers pairs and their orbital shapes in Sr_2IrO_4. The spin-orbit entangled nature of these quantum states is illustrated with colors; orange (blue) represent spin up (down) projection. **b**, Spectrum at **q**=(π/2, π/2) measured at three different x-ray incident angle ϕ. A, B, and C denote the energy positions of the three Kramers pairs illustrated in **a**. The scattering angle 2θ was kept within 5 degrees from 90°.

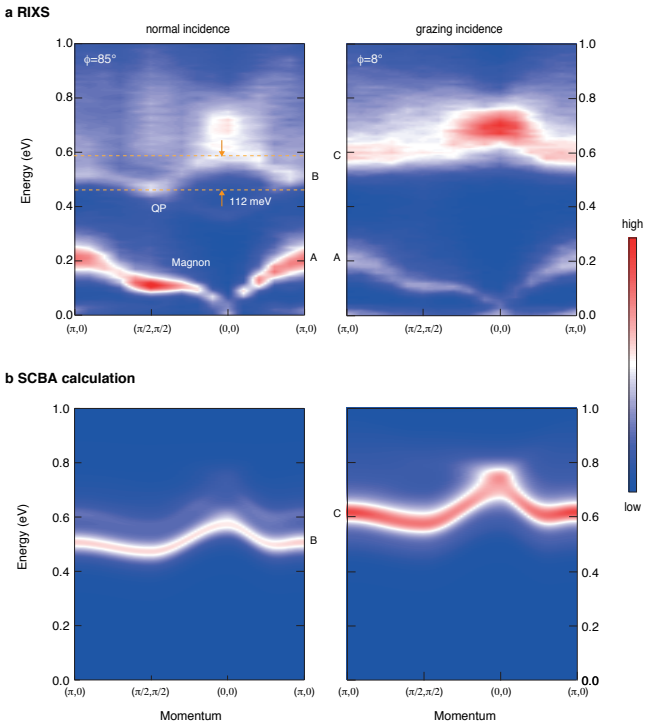

FIG. 3. **Selective mapping of the two exciton modes and their comparison to SCBA calculations. a**, Image plot of RIXS spectra measured along high symmetry lines in the normal and grazing incidence geometry. **b**, SCBA calculations using the parameters λ_{SO}= 382 meV, Δ_{BC}= 137 meV, $t_1 = J_1/2$ =30 meV, $t_2 = t_3$ = 7.6 meV, J_1 = 60 meV, J_2 = -20 meV, and J_3 = 15 meV. $t_{1,2,3}$ ($J_{1,2,3}$) denote first, second, and third nearest neighbor hoppings (magnetic couplings). λ_{SO} and Δ_{BC} are defined in fig. 2. The spectral functions obtained by SCBA calculations are convoluted with a Lorentzian function with 5 meV width.

hole-vs.-exciton analogy: a foreign object injected into a quantum Heisenberg antiferromagnet, be it a hole or an exciton, creates a string of flipped spins along its hopping path. This analogy, in principle, suggests that the dynamics of a particle moving in a magnetic medium can also be studied using the exciton. However, the energy resolution of RIXS used in the earlier study (≈130 meV) was insufficient to resolve the dispersion and the intrinsic linewidth of the two exciton modes associated with the two pairs of Kramers doublets in the j=3/2 manifold (Fig. 2a). In this Letter, we exploit the different orbital symmetries of the two exciton modes to selectively probe each mode, and with the much improved energy resolution (≈30 meV) offered by RIXS after recent developments, reveal their full dynamics.

Figure 2b shows the RIXS spectra measured at three different incident angles ϕ of x-ray while fixing momentum transfer at **q**=(π/2, π/2). The two exciton modes, labeled as peaks B and C, show strong modulations in intensity as a function of through the change in the incident and outgoing x-ray polarizations relative to the sample surface and thereby the RIXS matrix elements. In particular, the peak B is strongly enhanced (completely suppressed) by tuning ϕ to normal (grazing) incidence geometry. This strong matrix element effect enables selective mapping of B and C modes, as shown in Fig. 3a. While both B and C modes display rather similar dispersions, the B mode has much narrower linewidth (see Fig. 4c) partly due to the fact that it has lower excitation energy and thus has less phase space to decay into. With the two exciton modes disentangled, our high-resolution measurement yields for the B mode a bandwidth of 112 meV. This finding is consistent with the expectation that the bandwidth is on the scale of a few times the antiferromagnetic exchange coupling J of about 60 meV.[20] The global topology of the dispersions with minimum at **q**=(π/2, π/2) and maximum at the point precisely matches that measured for a hole in cuprates by ARPES,[9] which strongly supports the hole-vs.-exciton analogy.

We compare the experimental data to the spectral function of the effective t-J model calculated within the SCBA (Fig. 3b). For details, see Supplementary Information and Ref. 20. The calculation yields two modes, one of which is predominantly from the Kramers doublet with quantum numbers $|J{=}3/2,\ J_z{=}\pm 3/2\rangle$, while the other has mostly $|J{=}3/2,\ J_z{=}\pm 1/2\rangle$ character. Through an

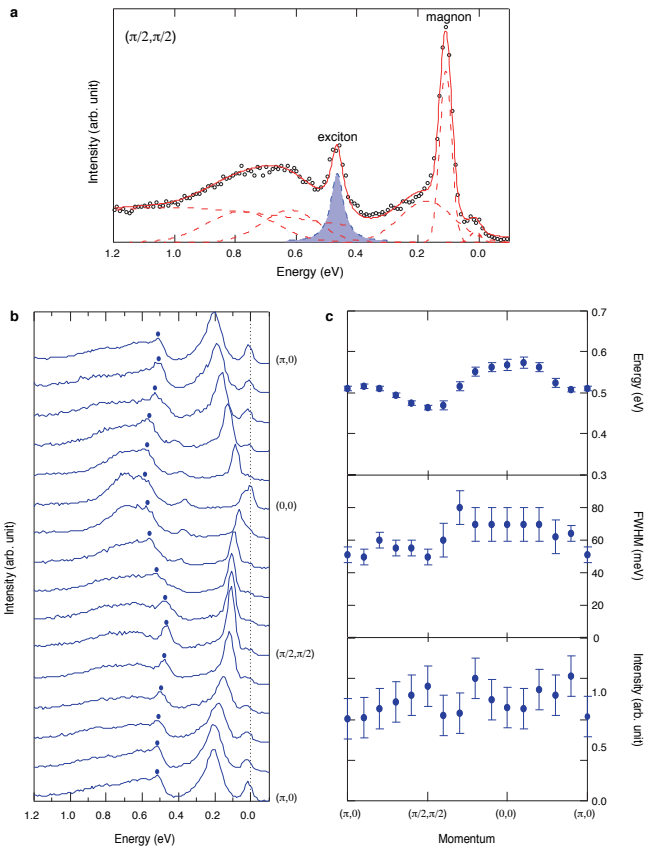

FIG. 4. **Exciton dynamics in Sr_2IrO_4.** **a**, RIXS spectrum at **q**=(π/2, π/2) (black open circles). The blue shaded peak corresponds to the exciton QP peak. The spectrum was fitted (red solid curve) using a Lorenzian lineshape for the exciton QP peak and Gaussian lineshapes for all other peaks (red dashed lines). The low energy features relative to exciton QP consist of elastic, single- and double-magnon peaks, and high-energy features the sum of C mode and background due to electron-hole continuum and incoherent part of B mode. **b**, Stack plot of the image plot in Fig. 2a, left panel. Oval symbols mark the energy position of the QP. In addition to the QP, a small peak with the dispersion minimum at the Γ point at E$\approx$0.37 eV is observed. A similar peak has been observed in a related material Na_2IrO_3 and attributed to a bound state at the edge of the particle-hole continuum.[42] **c**, Energy, width, and intensity of the QP peaks along high symmetry lines extracted from peak fitting as exemplified in **a**.

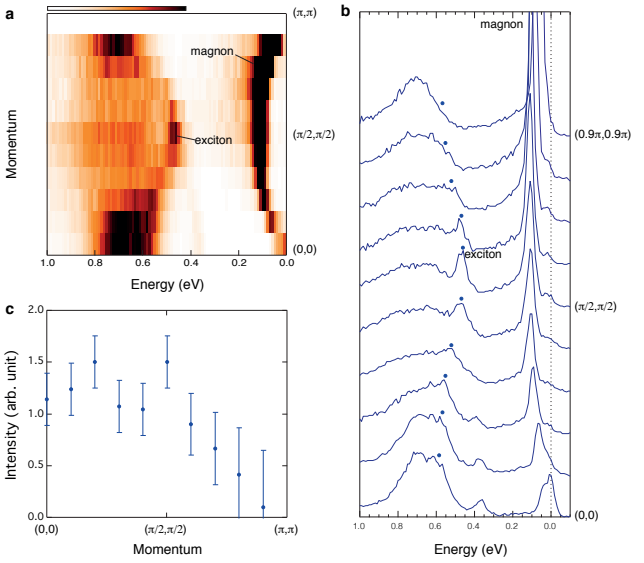

FIG. 5. **Asymmetric exciton QP intensity.** **a**, Image plot of RIXS spectra along (0,0)-(π,π) direction. **b**, Stack plot of the image plot in **a**. Oval symbols mark the energy position of the QP. **c**, Intensity of the QP peaks along (0,0)-(π,π) direction.

explicit calculation of the RIXS matrix elements, we find that their dependences on ϕ are such that the J_z=$\pm$1/2 states, with more in-plane components, are higher in energy (in the hole picture) than the J_z=$\pm$3/2 states. This level scheme is opposite to expectations based on perfectly cubic or c-axis elongated oxygen octahedra, but agrees with the results from non-resonant inelastic x-ray scattering,[29] electron spin resonance[30] and quantum chemistry calculations.[31] Taking a crystal field splitting Δ_{BC} of 137 meV and fixing all other parameters to values inferred from independent studies, the effective t-J model reproduces the gross features of the experimental spectra. Details are improved by including further neighboring hoppings, which are expected to be significant from sizable further neighbor magnetic couplings. With the parameters given in the Fig. 3b caption, we find an excellent agreement with the data in terms of the polarization dependence and the dispersion relations, confirming that the exciton dynamics is essentially captured by the effective t-J model.

Having justified the hole-vs.-exciton analogy, we now bring to light the key observation from the exciton spectra. The energy distribution curves, measured in the normal incidence geometry to highlight the B mode, reveal a very sharp exciton peak, most prominent at **q**=(π/2, π/2) (Fig. 4a) and resolved throughout most part of the Brillouin zone (Fig. 4b). We use a phenomenological Lorentzian lineshape to fit the spectra to extract the peak energy, width, and intensity, which are summarized in Fig. 4c. Remarkably, the peak width is as narrow as $\approx$50 meV (of which 30 meV is contributed by the experimental resolution), much narrower than that of the sharpest peak ($\sim$200 meV) in the hole spectral function measured by ARPES for the same material.[17,32] The peak width is also much smaller than its total bandwidth ($\approx$112 meV), which establishes the exciton as a propagating mode in a solid, or a QP. More importantly, our observation of an excitonic QP establishes hard evidence that a particle can propagate coherently through a quantum antiferromagnet. This raises a fundamental question: why is a QP absent for the single hole excitation?

Thus far we have focused on the similarity between the dynamics of a hole and an exciton. Let us now discuss some important differences. A hole is a charge monopole

and its sudden creation in the ARPES process leads to deformation of the surrounding ionic oxygen cage, which results in a strong hole-lattice coupling detrimental for the hole propagation. Further, a hole interacts with charged impurities always present and poorly screened in an insulator. Both of these effects have been shown to strongly damp or wash out sharp QPs,[33–35] thereby significantly redistributing the hole spectral function. In fact, most likely for these reasons, for a quasi-one-dimensional system Sr_2CuO_3 in which the phenomenon of spin-charge separation is established,[36] ARPES measures much-broadened spectra[37,38] of the theoretically predicted sharp edge-singularity in the exactly soluble model. By contrast, a charge-neutral exciton with a quadrupole moment should couple much more weakly to the lattice and is not subject to long-range Coulomb forces due to impurities. Thus, an exciton avoids these 'side effects' and reveals the intrinsic dynamics of the t-J model that have remained elusive for the past several decades.

Our central message is that the unprecedentedly narrow linewidth of the QP allows a direct access into the nature of a QP living in the background of ordered spins, and thus that it allows direct verification of a class of theories that predict a finite quasiparticle residue in the Mott insulating phase, which has thus far remained inconclusive in the apparent absence of a QP in the hole channel. For instance, the observed exciton intensity can be compared with that calculated in theoretical models on a quantitative level. Figures 5a and 5b show the exciton dispersion along (0,0)-(π,π) direction. The dispersion is symmetric with respect to ($\pi/2$,$\pi/2$) point on the magnetic zone boundary, but the intensities inside and outside of the magnetic zone differ significantly (Fig. 5c); the exciton QP displays a steep drop in intensity as ($\pi/2$,$\pi/2$) is crossed. This is a generic feature predicted for a hole in a t-J model within a SCBA approach[39] and indirectly inferred from ARPES measurements on cuprates,[40] which possibly accounts for the Fermi arc observed in the doped case as due to the strongly suppressed shadow band intensity. Although some deviations from the cuprate physics might have been expected on general grounds due to fundamentally different nature of a hole and an exciton, and material specific differences between Sr_2IrO_4 and cuprates, the striking agreement down to a level of fine details with theories constructed for hole dynamics in cuprates demonstrates excellent parallel between the low-energy physics of Sr_2IrO_4 and the cuprates.

Methods Single crystals of Sr_2IrO_4 were grown by the flux method. The sample was mounted in a displex closed-cycle cryostat and measured at 15 K. The RIXS measurements were performed using the MERIX spectrometer at the 30-ID beamline[41] of the Advanced Photon Source. X-rays were monochromatized to a bandwidth of 15 meV, and focused to have a beam size of 45(H)×30(V) μm^2. A horizontal scattering geometry was used with the incident photon polarization. A Si (844) diced spherical analyzer with 4 inch radius and a position-sensitive silicon microstrip detector were used in the Rowland geometry. The overall energy resolution of the MERIX spectrometer at the Ir L_3 edge was 30 meV, as determined from the full-width-half-maximum of the elastic peak.

References

[1] Landau, L. D. The theory of a Fermi liquid. Sov. Phys. JETP **3**, 920-925 (1957).

[2] Norman, M. R. Unconventional superconductivity, Prepreint at http://arxiv.org/pdf/1302.3176v1

[3] Stewart, G. R. Non-Fermi-liquid behavior in d- and f-electron metals, Rev. Mod. Phys. **73**, 797-848 (2001).

[4] Lee, P. A., Nagaosa, N., Wen, X.-G. Doping a Mott insulator: Physics of high-temperature superconductivity. Rev. Mod. Phys. **78**, 17-85 (2001).

[5] Schmitt-Rink, S., Varma, C. M., Ruckenstein, A. E. Spectral function of holes in a quantum antiferromagnet. Phys. Rev. Lett. **60**, 2793 (1988).

[6] Kane, C. L, Lee, P. A., Read, N. Motion of a single hole in a quantum antiferromagnet. Phys. Rev. B **39**, 6880 (1989).

[7] Duffy, D., Nazarenko, A., Haas, S., Moreo, A., Riera, J., Dagotto, E. Hole-doping evolution of the quasiparticle band in models of strongly correlated electrons for the high-Tc cuprates. Phys. Rev. B **56**, 5597 (1997).

[8] Eder, R., Ohta, Y., Sawatzky, G. A. Doping-dependent quasiparticle band structure in cuprate superconductors. Phys. Rev. B **55**, R3414 (1996).

[9] Wells, B. O., Shen, Z. -X., Matsuura, A., King, D. M., Kastner, M. A., Greven, M., Birgeneau, R. J. E versus k relations and many body effects in the model insulating copper oxide $Sr_2CuO_2Cl_2$. Phys. Rev. Lett. **74**, 964967 (1995).

[10] Tohyama, T., Maekawa S. Angle-resolved photoemission in high T_C cuprates from theoretical viewpoints. Supercond. Sci. Technol. **13**, R17R32 (2000).

[11] Shen, K. M., Ronning, F., Lu, D. H., Lee, W. S., Ingle, N. J. C., Meevasana, W., Baumberger, F., Damascelli, A., Armitage, N. P., Miller, L. L., Kohsaka, Y., Azuma, M., Takano, M., Takagi, H., Shen, Z.-X. Missing quasiparticles and the chemical potential puzzle in the doping evolution of the cuprate superconductors. Phys. Rev. Lett. **93**, 267002 (2004).

[12] Ye, C., Cai, P, Yu, R., Zhou, X., Ruan, W., Liu, Q., Jin, C., Wang, Y. Visualizing the atomic-scale electronic structure of the $Ca_2CuO_2Cl_2$ Mott insulator. Nat. Commun. **4**. 1365 (2013).

[13] Anderson, P. W. Luttinger-liquid behavior of the normal metallic state of the 2D Hubbard model. Phys. Rev. Lett. **64**, 1839 (1990).

[14] Laughlin, R. B. Evidence for Quasiparticle Decay in Photoemission from Underdoped Cuprates. Phys. Rev. Lett. **79**, 1726 (1997).

[15] Sheng, D. N., Chen, Y. C., Weng, Z. Y. Phase string ef-

fect in a doped antiferromagnet. Phys. Rev. Lett. **77**, 5102 (1996).

[16] Anderson, P. W., Lee, P. A., Randeria, M., Rice, T. M., Trivedi, N, Zhang, F. C. The physics behind high-temperature superconducting cuprates: the 'plain vanilla' version of RVB. J. Phys.: Condens. Matter **16**, R755 (2004).

[17] Kim, B. J., Jin, H., Moon, S. J., Kim, J.-Y, Park, B.-G., Leem, C. S., Yu, J., Noh, T.W., Kim, C., Oh, S.-J., Park, J.- H., Durairaj, V., Cao, G., Rotenberg, E. Novel J_{eff} =1/2 Mott state induced by relativistic spin-orbit coupling in Sr_2IrO_4. Phys. Rev. Lett. **101**, 076402 (2008).

[18] Jackeli, G., Khaliullin, G. Mott insulators in the strong spin-orbit coupling limit: from Heisenberg to a quantum compass and Kitaev models. Phys. Rev. Lett. **102**, 017205 (2009).

[19] Kim, B. J., Ohsumi, H., Komesu, T., Sakai, S., Morita, T., Takagi, H., Arima, T. Phase-sensitive observation of a spin-orbital Mott state in Sr_2IrO_4. Science **323**, 1329-1332 (2009).

[20] Kim, J., Casa, D., Upton, M. H., Gog, T., Kim, Y.-J., Mitchell, J. F., van Veenendaal, M., Daghofer, M., van den Brink, J., Khaliullin, G., Kim, B. J. Magnetic excitation spectra of Sr_2IrO_4 probed by resonant inelastic x-ray scattering: Establishing links to cuprate superconductors. Phys. Rev. Lett. **108**, 177003 (2012).

[21] Fujiyama, S., Ohsumi, H., Komesu, T., Matsuno, J., Kim, B. J., Takata, M., Arima, T., Takagi, H., Two-dimensional Heisenberg behavior of J_{eff}=1/2 isospins in the paramagnetic state of the spin-orbital Mott insulator Sr_2IrO_4, Phys. Rev. Lett. **108**, 247212 (2012).

[22] Crawford, M. K., Subramanian, M. A., Harlow, R. L., Fernandez-Baca, J. A., Wang, Z. R., Johnston, D. C. Structural and magnetic studies of Sr_2IrO_4. Phys. Rev. B **49**, 9198-9201 (1994).

[23] Wang, F., Senthil, T. Twisted Hubbard model for Sr_2IrO_4: Magnetism and possible high temperature superconductivity. Phys. Rev. Lett. **106**, 136402 (2011).

[24] Martins, C., Aichhorn, M., Vaugier, L., Biermann, S. Reduced effective spin-orbital degeneracy and spin-orbital ordering in paramagnetic transition-metal oxides: Sr_2IrO_4 versus Sr_2RhO_4. Phys. Rev. Lett. **107**, 266404 (2011).

[25] Arita, R., Kune, J., Kozhevnikov, A. V., Eguiluz, A. G., Imada, M. Ab initio studies on the interplay between spin-orbit interaction and coulomb correlation in Sr_2IrO_4 and Ba_2IrO_4. Phys. Rev. Lett. **108**, 086403 (2012).

[26] Hsieh, D., Mahmood, F., Torchinsky, D. H., Cao, G., Gedik, N. Observation of a metal-to-insulator transition with both Mott-Hubbard and Slater characteristics in Sr_2IrO_4 from time-resolved photocarrier dynamics. Phys. Rev. B **86**, 035128 (2012).

[27] Li, Q., Cao, G., Okamoto, S., Yi, J., Lin W., Sales, B. C., Yan, J., Arita, R., Kunes, J., Kozhevnikov, A. V., Eguiluz, A. G., Imada, M., Gai, Z., Pan, M., Mandrus, D. G. Microscopic and spectroscopic evidence for a Slater metal-Insulator transition in Sr_2IrO_4. Preprint at http://arxiv.org/abs/1303.7265.

[28] Yamasaki, A. et al. Bulk nature of layered perovskite iridates beyond the Mott scenario: An approach from bulk sensitive photoemission study. Phys. Rev. B **89**, 121111(R) (2014).

[29] Fujiyama, S., Ohsumi, H., Ohashi, K., Hirai, D., Kim, B. J., Arima, T., Takata, M., Takagi, H. Spin and orbital contributions to magnetically ordered moments in 5d layered perovskite Sr_2IrO_4. Phys. Rev. Lett. **112**, 016405 (2014).

[30] Bahr, S., Alfonsov, A., Jackeli, G., Khaliullin, G., Matsumoto, A., Takayama, T., Takagi, H., Bchner, B., Kataev, V. Low energy magnetic excitations in the spin-orbital Mott insulator Sr_2IrO_4. Preprint at http://arxiv.org/abs/1312.4847.

[31] Katukuri, V. M., Stoll, H., van den Brink J., Hozoi, L. Ab initio determination of excitation energies and magnetic couplings in correlated quasi-two-dimensional iridates. Phys. Rev. B **85**, 220402(R) (2012).

[32] Wang, Q., Cao. Y, Waugh, J. A., Park, S. R., Qi, T. F., Korneta, O. B., Cao, G., Dessau, D. S. Dimensionality-controlled Mott transition and correlation effects in single-layer and bilayer perovskite iridates. Phys. Rev. B **87**, 245109 (2013).

[33] Mishchenko, A. S., Nagaosa, N. Electron-phonon coupling and a polaron in the t-J model: from weak to the strong coupling regime. Phys. Rev. Lett. **93**,036402 (2004).

[34] Chen, W., Khaliullin, G., Sushkov, O. P. Coulomb disorder effects on angle-resolved photoemission and nuclear quadrupole resonance spectra in cuprates. Phys. Rev. B **80**, 094519 (2009).

[35] King, P. D. C., Takayama, T., Tamai, A., Rozbicki, E., Walker, S. M., Shi, M., Patthey, L., Moore, R. G., Lu, D., Shen, K. M., Takagi, H., Baumberger, F. Spectroscopic evidence for polaronic behaviour of the strong spin-orbit insulator $Sr_3Ir_2O_7$. Phys. Rev. B **87**, 241106(R) (2013).

[36] Zaliznyak, I. A., Woo, H., Perring, T. G., Broholm, C. L., Frost, C. D., Takagi, H. Spinons in the strongly correlated copper oxide chains in $SrCuO_2$. Phys. Rev. Lett. **93**, 087202 (2004).

[37] Kim, C. Matsuura, A. Y., Shen, Z.-X., Motoyama, N., Eisaki, H., Uchida, S., Tohyama, T., Maekawa, S. Observation of spincharge separation in one-dimensional $SrCuO_2$. Phys. Rev. Lett. **77**, 40544057 (1996).

[38] Kim, B. J., Koh, H., Rotenberg, E., Oh, S.-J., Eisaki, H., Motoyama, N., Uchida, S., Tohyama, T., Maekawa, S., Shen, Z.-X., Kim, C. Distinct spinon and holon dispersions in photoemission spectral functions from one-dimensional $SrCuO_2$. Nat. Phys. **2**, 397401 (2006).

[39] Sushkov, O. P., Sawatzky, G. A., Eder, R., Eskes, H. Hole photoproduction in insulating copper oxide. Phys. Rev. B **56**, 11769 (1997).

[40] LaRosa, S., Vobornik, I., Zwick, F., Berger, H., Grioni, M., Margaritondo, G., Kelley, R. J., Onellion M., Chubukov, A. Electronic structure of CuO_2 planes: From insulator to superconductor. Phys. Rev. B **56**, R525 (1997).

[41] Gog, T., Casa, D. M., Said, A. H., Upton, M. H., Kim, J., Kuzmenko, I., Huang, X., Khachatryan, R. Spherical analyzers and monochromators for resonant inelastic hard X-ray scattering: a compilation of crystals and reflections. J. Synchrotron Rad. **20** 74-79 (2013).

[42] Gretarsson, H., Clancy, J. P., Liu, X., Hill, J. P., Bozin, E., Singh, Y., Manni, S., Gegenwart, P., Kim, J., Said, A. H., Casa, D., Gog, T., Upton, M. H., Kim, H.-S., Yu, J., Katukuri, V. M., Hozoi, L., van den Brink, J., Kim, Y.-J. Crystal-field splitting and correlation effect on the electronic structure of A_2IrO_3. Phys. Rev. Lett. **110**, 076402 (2013).

Supplementary Note 1

The effective t-J model and the calculation of exciton spectra within self-consistent Born approximation

The theoretical modeling is based on the observation that propagation of an orbital excitation in a Mott insulator can be mapped onto a single hole moving in the system,[1,2] as illustrated in Fig. 1. We extend here the approach used in Ref. 1 by employing a more accurate technique, the self-consistent Born approximation (SCBA).[3] In contrast to the second-order perturbation theory used previously,[1] which is valid for exciton hopping small compared to magnetic interactions, it contains diagrams to all orders of the hopping, i.e, in the coupling between exciton motion and the magnetic background. Together with the much increased experimental resolution, the use of the SCBA rather than perturbation theory allows a more quantitative comparison of theory and experiment. We find that a good description of the data can be obtained with spin-orbit coupling $\lambda = 382$ meV, crystal-field splitting $\Delta = -188$ meV (in the notation of Ref. 4), magnetic couplings fitted to the magnon dispersion[1] and by allowing for longer-range hopping of the spin-orbit excitation. As mentioned in the main text, these parameter values are well supported by other experiments and ab initio methods – with the exception of the longer-range hoppings, which can only be investigated via precise measurement of the exciton propagation, as done here.

The SCBA is a diagrammatic approach that describes the antiferromagnetic (AFM) background with linear spin-wave theory. The diagrams describing coupling of the moving hole or exciton to the (pseudo-)spin background are those without crossing magnon lines, an approximation that has been shown to be valid as the leading crossing diagrams drop out for symmetry reasons.[5] The method has been extensively used to investigate hole motion in an AFM and has been used to discuss propagation of an orbital excitation[6]. In contrast to second-order perturbation theory, it allows to describe incoherent spectral weight as well as coherent quasi-particle motion. Nevertheless, it underestimates quantum fluctuations of the magnetic background and higher-order vertex corrections may become more relevant for a hopping of a similar size as exchange coupling.

The A, B and C modes all mix spin and orbital of the $5d$ wave functions, depending on spin-orbit coupling and crystal-field splitting Δ between the xy and xz/yz orbitals. The low-energy A states are then given by $|\mathrm{A}_\sigma\rangle = \sin\theta|\tau=0;\sigma\rangle - \cos\theta|\tau=\sigma;-\sigma\rangle$, where $\sigma = \pm 1$ denotes the pseudospin and $\tau = 0, \pm 1$ the orbital angular momentum and θ is given by $\tan 2\theta = 2\sqrt{2}\lambda/(\lambda - 2\Delta)$.[4] The higher-energy modes B and C, which we focus on

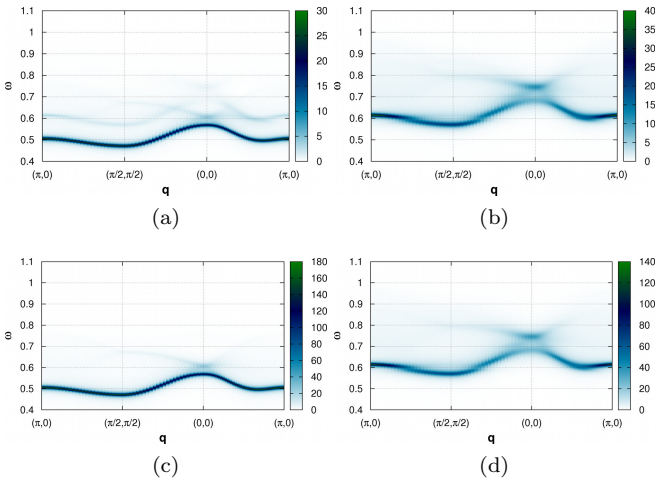

FIG. S1. Theoretical spectra for a scattering geoemtry with (a) ϕ=90° and (b) ϕ=0°. In (c) and (d), the weight for the two doublets B and C is shown, i.e. $-\mathcal{I}G^{\mathrm{BB}}$ in (c) and $-\mathcal{I}G^{\mathrm{CC}}$ in (d). The parameters used were $\lambda = 382$ meV, $\Delta = -188$ meV, $W_1 = J_1/2 = 30$ meV, $W_2 = W_3 = 7.6$ meV, $J_1 = 60$ meV, $J_2 = -20$ meV, and $J_3 = 15$ meV. Imaginary part used in the SCBA was $\delta = 5$ meV.

here, are given by

$$|\mathrm{B}_\sigma\rangle = |\tau=\sigma;\sigma\rangle, \quad \text{and} \tag{1}$$
$$|\mathrm{C}_\sigma\rangle = \cos\theta\ |\tau=0;\sigma\rangle + \sin\theta\ |\tau=\sigma;-\sigma\rangle\ . \tag{2}$$

The energy cost of exciting a hole from the A into the B or C doublets is given by

$$E^{\mathrm{C}} = \frac{3\lambda}{2}\sqrt{1 - \frac{4\Delta}{9\lambda} + \frac{4\Delta^2}{9\lambda^2}}$$
$$E^{\mathrm{B}} = \frac{\Delta}{2} + \frac{3\lambda}{4} + \frac{3\lambda}{4}\sqrt{1 - \frac{4\Delta}{9\lambda} + \frac{4\Delta^2}{9\lambda^2}}\ . \tag{3}$$

The splitting between A, B and C modes observed in the RIXS data can be reproduced by taking spin-orbit coupling $\lambda = 382$ meV and a crystal-field splitting $\Delta = -188$ meV, yielding $\theta \approx 0.15\pi$. The sign of Δ is here chosen as in Ref. 4, i.e., it is positive for elongated octahedra and negative for shortened ones, if one considers a simple point-charge model. However, we find that in order to reproduce the order of the B and C modes as seen in experiment, and consistent with first-principle calculations[7] and other experiments[8], $\Delta < 0$ has to be chosen for Sr_2IrO_4. In the notation used in the main text, the resulting splitting $E^{\mathrm{C}} - E^{\mathrm{B}} = \Delta_{\mathrm{BC}} = 137.4$ meV between B and C levels has the sign opposite to that of Δ, i.e., it is here positive.

As discussed in Ref. 1, the orbital excitation moves via a superexchange process with the matrix element

$$W^{\beta\gamma}_{x/y} = -\frac{2t_{\mathrm{AA}}}{U'}\begin{pmatrix} t_{BB} & \pm t_{\mathrm{BC}} \\ \pm t_{\mathrm{BC}} & t_{\mathrm{CC}} \end{pmatrix} = \tag{4}$$
$$= -\frac{J}{2}\frac{U}{U'}\begin{pmatrix} t_{BB}/t_{\mathrm{AA}} & \pm t_{\mathrm{BC}}/t_{\mathrm{AA}} \\ \pm t_{\mathrm{BC}}/t_{\mathrm{AA}} & t_{\mathrm{CC}}/t_{\mathrm{AA}} \end{pmatrix} = -W_1\tau^{\alpha\beta}_{x/y}$$

along the x and y directions, respectively. $t_{\alpha,\beta}$ are here the direct hopping elements for the three Kramers-doublets A, B, and C. U' is the Coulomb repulsion between two electrons on the same site, but in different orbitals. Since $SU(2)$ symmetry pseudospin excitations of the A sector indicate small Hund's rule coupling, it is not expected to differ much from the intraorbital repulsion U and we take here $U' = U$. The overall factor scaling the propagation is then $W_1 = \frac{J}{2} \approx 30$ meV. To distinguish them more clearly from the bare hopping elements t referring to electron motion, effective exciton hoppings are denoted by W in this supplementary material, following earlier work.[1] The bare hopping elements entering (4) depend on the composition of the states as

$$t_{\rm AA} = \frac{3}{4} - \frac{\cos 2\theta}{4}, \qquad t_{\rm BB} = \frac{1}{2} \qquad (5)$$
$$t_{\rm CC} = \frac{3}{4} + \frac{\cos 2\theta}{4}, \qquad t_{\rm BC} = \frac{\sin\theta}{2} \ .$$

As the excitonic hopping is a superexchange process, it scales with the magnetic exchange J, see (4). In Sr_2IrO_4, nearest-neighbor exchange is here taken as $J = 60$ meV. Longer-range couplings are also present and sizable with $\approx 15 - 20$ meV, analogously, we introduce longer-range exciton hoppings $W_2^{\beta\gamma}$ and $W_3^{\beta\gamma}$ for second and third neighbors. For simplicity, they are assumed to be identical for the B and C doublet with $W_{2/3}^{\rm BC} = 0$, leaving us with two parameters $W_2^{\rm BB} = W_2^{\rm CC} = W_2$ and $W_3^{\rm BB} = W_3^{\rm CC} = W_3$. They are adjusted to fit the quasiparticle dispersion, like longer-range hoppings in the case of ARPES. Exciton hopping and magnetic background together are thus described by an effective t-J model, where both hopping and magnetic exchange are included up to third neighbors. In order to make the analogy to cuprates more transparent, W_1, W_2 and W_3 are denoted by t_1, t_2, and t_3 in the main text. One difference to the t-J model used to describe hole motion in an antiferromagnet is the orbital index of the exciton. Moreover, hopping W and magnetic coupling J are of the same order of magnitude, as they share the same origin, superexchange.

In order to treat this problem, we follow a route extensively used to describe hole propagation in the t-J model, where the AFM order is treated in linear spin-wave approximation. For the case with only nearest-neighbor terms and for a single excited-orbital mode, it has been used to discuss propagation of an orbital excitation[6]. The Hamiltonian is Fourier-transformed into momentum space and a Bogoliubov transformation is applied to the magnetic part. The magnetic energy becomes

$$H_{\rm mag} = \sum_{\mathbf{q}} \omega_{\mathbf{q}} a_{\mathbf{q}}^\dagger a_{\mathbf{q}} \qquad (6)$$

where $a_{\mathbf{q}}$ ($a_{\mathbf{q}}^\dagger$) annihilates(creates) a magnon with momentum $\mathbf{q}$, with a magnon energy

$$\omega_{\mathbf{q}} = \sqrt{{\rm A}_{\mathbf{q}}^2 - {\rm B}_{\mathbf{q}}^2} \ , \qquad (7)$$

and coefficients

$${\rm A}_{\mathbf{q}} = 2(J_1 - J_2 - J_3 + J_2\cos q_x \cos q_y) + J_3(\cos 2q_x + \cos 2q_y),$$
$${\rm B}_{\mathbf{q}} = J_1(\cos q_x + \cos q_y) \ . \qquad (8)$$

The magnetic couplings are chosen as $J_1 = 60$ meV, $J_2 = -20$ meV, and $J_3 = 15$ meV, in order to describe the 'magnon' excitations of the pseudospin-1/2 checkerboard order.[1] Nearest-neighbor hopping moves the exciton, i.e., the hole in the AFM background from one sublattice of the AFM order to the other and thereby couples to the magnetic background. It can be written as

$$H_{\rm NN} = -\frac{zW_1}{\sqrt{N}} \sum_{\mathbf{k},\mathbf{q},\alpha,\beta} \left[M_{\mathbf{k},\mathbf{q}}^{\alpha\beta} X_{\alpha\mathbf{k}}^\dagger X_{\beta\mathbf{k}-\mathbf{q}} a_{\mathbf{q}} + h.c. \right] , \quad (9)$$

where N is the number of sites and $z = 4$ the coordination number. $X_{\alpha\mathbf{k}}^\dagger$ and $X_{\beta\mathbf{k}}$ create and annihilate the exciton at momentum $\mathbf{k}$ and orbital index α. The orbital and direction dependence of Eq. (4) was absorbed into the orbital-dependent vertex

$$M_{\mathbf{k},\mathbf{q}}^{\alpha\beta} = |\tau^{\alpha\beta}|(u_{\mathbf{q}}\gamma_{\mathbf{k}-\mathbf{q}}^{\alpha\beta} + v_{\mathbf{q}}\gamma_{\mathbf{k}}^{\alpha\beta}) \qquad (10)$$

via

$$\gamma_{\mathbf{k}}^{\alpha\beta} = \frac{1}{2} \begin{pmatrix} (\cos k_x + \cos k_y) & (\cos k_x - \cos k_y) \\ (\cos k_x - \cos k_y) & (\cos k_x + \cos k_y) \end{pmatrix} ; \quad (11)$$

Bogoliubov factors $u_{\mathbf{q}}$ and $v_{\mathbf{q}}$ are given by the relations

$$u_{\mathbf{q}} = \frac{1}{\sqrt{2}} \sqrt{\frac{{\rm A}_{\mathbf{q}}}{\omega_{\mathbf{q}}} + 1}, \quad v_{\mathbf{q}} = -\frac{{\rm sgnB}_{\mathbf{q}}}{\sqrt{2}} \sqrt{\frac{{\rm A}_{\mathbf{q}}}{\omega_{\mathbf{q}}} - 1} \ . \quad (12)$$

Second- and third-neighbor hoppings W_2 and W_3, in contrast, allow the exciton to move within one sublattice of the AFM background and consequently do not disturb the the magnetic order. Together with the onsite energies $E^{\rm B}$ and $E^{\rm C}$ reflecting the energy cost of exciting a hole from the A into the B or C doublets, see (3), they add a 'free' non-interacting exciton Hamiltonian: [9]

$$H_0 = -\frac{1}{\sqrt{N}} \sum_{\mathbf{q},\alpha} \epsilon_{\mathbf{q}}^\alpha X_{\alpha\mathbf{q}}^\dagger X_{\alpha\mathbf{q}} \quad \text{with} \qquad (13)$$
$$\epsilon_{\mathbf{q}}^\alpha = E^\alpha - 4W_2 \cos\mathbf{q}_x \cos\mathbf{q}_y - 2W_3(\cos 2\mathbf{q}_x + \cos 2\mathbf{q}_y).$$

The full Hamiltonian $H_0 + H_{\rm NN} + H_{\rm mag}$ is then treated using the self-consistent Born approximation,[3] a diagrammatic approach where the self energy is expressed as

$$\Sigma^{\alpha\beta}(\mathbf{k},\omega) = -\frac{z^2W^2}{N} \sum_{\mathbf{q},\gamma,\gamma'} M_{\mathbf{k},\mathbf{q}}^{\alpha\gamma} G^{\gamma\gamma'}(\mathbf{k}-\mathbf{q}, \omega-\omega_{\mathbf{q}}) M_{\mathbf{k},\mathbf{q}}^{\gamma'\beta}, \qquad (14)$$

with the interacting Green's function conveniently expressed via its inverse matrix G^{-1} as

$$\left\{G^{-1}(\mathbf{q},\omega)\right\}^{\alpha\alpha} = \omega + i\delta - \epsilon_{\mathbf{q}}^\alpha - \Sigma^{\alpha\alpha}(\mathbf{q},\omega), \qquad (15)$$
$$\left\{G^{-1}(\mathbf{q},\omega)\right\}^{\alpha\beta\neq\alpha} = -\Sigma^{\alpha\beta}(\mathbf{q},\omega).$$

The small imaginary part $i\delta$ was here chosen as $\delta = 5$ meV. Many of the diagrams neglected in thin non-crossing approximation drop out for the square-lattice Néel state, however, it underestimates quantum fluctuations of the background.

The resonant inelastic x-ray scattering (RIXS) spectra can be simulated from the spectral density $-\mathcal{I}G^{\alpha\beta}(\mathbf{q},\omega)$ with proper consideration of the factors arising from the scattering geometry. The RIXS intensity can be expressed as

$$I = -|\beta|^2\mathcal{I}G^{\mathrm{BB}}(\mathbf{q},\omega) - |\gamma|^2\mathcal{I}G^{\mathrm{CC}}(\mathbf{q},\omega) - \beta^*\gamma\mathcal{I}G^{\mathrm{BC}}(\mathbf{q},\omega) - \beta\gamma^*\mathcal{I}G^{\mathrm{CB}}(\mathbf{q},\omega) \tag{16}$$

where coefficients β and γ are obtained in a similar manner as in Ref. 1, extended here to account for the deviations from the cubic limit. They depend on incoming and outgoing polarizations ϵ and ϵ' as well as on the spin of the excited particle. As the spin does not enter the calculation of the spectral weight and the outgoing polarization ϵ' is not analyzed, we average over both. The matrix elements are given by

$$\beta_{\sigma,\sigma} = \frac{1}{2}\cos\theta_0\cos(\theta-\theta_0)(Q_2 + i\sigma T_z), \tag{17}$$

$$\beta_{\sigma,-\sigma} = \frac{1}{2\sqrt{2}}\sin\theta_0\cos(\theta-\theta_0)\left[-\sigma(T_y+P_y) + i(T_x - P_x)\right], \tag{18}$$

$$\gamma_{\sigma,\sigma} = \frac{\sin(2\theta_0-2\theta)}{4\sqrt{3}}(\sqrt{2}Q_1 + Q_3) + \frac{\sqrt{3}\sin 2\theta}{4}Q_3 + i\sigma\frac{1}{4}[\sin 2\theta - \sin(2\theta_0-2\theta)]P_z \tag{19}$$

$$\gamma_{\sigma,-\sigma} = \frac{1}{2\sqrt{2}}\left[\sigma(T_y - \cos 2\theta P_y) + i(T_x + \cos 2\theta P_x)\right] \tag{20}$$

where θ_0 is the 'mixing angle' in the cubic limit, which applies to the oxygen levels that are not affected by octahedral distortions and is given by $\tan 2\theta_0 = 2\sqrt{2}$. Further,

$$\vec{P} = \epsilon' \times \epsilon \tag{21}$$

$$Q_1 = \sqrt{2/3}\epsilon\cdot\epsilon' \tag{22}$$

$$Q_2 = \epsilon'_y\epsilon_y - \epsilon'_x\epsilon_x, \tag{23}$$

$$Q_3 = \frac{1}{\sqrt{3}}(\vec{\epsilon'}\cdot\vec{\epsilon} - 3\epsilon'_z\epsilon_z), \tag{24}$$

$$T_x = \epsilon'_y\epsilon_z + \epsilon'_z\epsilon_y, \tag{25}$$

$$T_y = \epsilon'_x\epsilon_z + \epsilon'_z\epsilon_x, \tag{26}$$

$$T_z = \epsilon'_y\epsilon_x + \epsilon'_x\epsilon_y. \tag{27}$$

We approximate the normal incidence scattering geometry in Fig. 2b by taking ϕ=90°. The resulting spectra are shown in Supplementary Fig. 1a. A comparison to the orbital-resolved spectra shown in Supplementary Figs. 1c and 1d reveals that the spectral weight is dominated by the B doublet. For the ϕ=0° geometry the β-factors cancel out and the resulting spectrum, shown in Supplementary Fig. 1b, shows only the higher-energy C mode.

Supplementary References

[1] J. Kim, D. Casa, M. Upton, T. Gog, Y.-J. Kim, J. Mitchell, M. Van Veenendaal, M. Daghofer, J. van den Brink, G. Khaliullin, and B. Kim, Phys. Rev. Lett. **108**, 177003 (2012).

[2] K. Wohlfeld, M. Daghofer, S. Nishimoto, G. Khaliullin, and J. van den Brink, Phys. Rev. Lett. **107**, 147201 (2011).

[3] S. Schmitt-Rink, C. Varma, and A. Ruckenstein, Phys. Rev. Lett. **60**, 2793 (1988).

[4] G. Jackeli and G. Khaliullin, Phys. Rev. Lett. **102**, 017205 (2009).

[5] Z. Liu and E. Manousakis, Phys. Rev. B 45, 2425 (1992).

[6] K. Wohlfeld, M. Daghofer, G. Khaliullin, and J. van den Brink, J. Phys.: Conf. Ser. **391**, 012168 (2012).

[7] V. M. Katukuri, H. Stoll, J. van den Brink J., and L. Hozoi, Phys. Rev. B **85**, 220402(R) (2012).

[8] S. Fujiyama *et al.*, arXiv:1308.0923; S. Bahr *et al.*, private communication.

[9] J. Bała, A. M. Oleś, and J. Zaanen, Phys. Rev. B **52**, 4597 (1995).